J. Phys.: Condens. Matter **24** (2012) 236004 (8pp) doi:10.1088/0953-8984/24/23/236004

The magnetic structure of EuPdSn

P Lemoine[1], J M Cadogan[1], D H Ryan[2] and M Giovannini[3,4]

[1] Department of Physics and Astronomy, University of Manitoba, Winnipeg, MB, R3T 2N2, Canada
[2] Physics Department and Centre for the Physics of Materials, McGill University, Montreal, QC, H3A 2T8, Canada
[3] Dipartimento di Chimica e Chimica Industriale, Università di Genova, Via Dodecaneso 31, 16146 Genova, Italy
[4] SPIN-CNR, Corso Perrone 24, 16152 Genova, Italy

E-mail: dhryan@physics.mcgill.ca

Received 24 February 2012, in final form 20 April 2012
Published 10 May 2012
Online at stacks.iop.org/JPhysCM/24/236004

Abstract
The TiNiSi-type structure, antiferromagnetic ordering and divalent state of europium in EuPdSn have been confirmed by neutron powder diffraction. The Néel temperature is 16.2(3) K. The magnetic diffraction peaks can be indexed with a propagation vector $\mathbf{k} = [0,\ 0.217,\ q_z]$ ($q_z \leq 0.02$) at 13.2 K, and $\mathbf{k} = [0,\ 0.276,\ 0]$ at 3.6 K, indicating an incommensurate antiferromagnetic structure at both temperatures. At 13.2 K, the best refinement is obtained with a sinusoidally modulated magnetic structure and europium magnetic moments oriented in the (a, b) plane with an azimuthal angle ϕ of 66(4)°relative to the a-axis. By 3.6 K, the magnetic structure of EuPdSn has transformed to an (a, b) planar helimagnetic structure (a 'flat spiral').

(Some figures may appear in colour only in the online journal)

1. Introduction

Europium, ytterbium and cerium compounds show a great variety of anomalous physical properties due to the different characters of their f-electrons [1, 2]. The ternary equiatomic RTX intermetallic compounds (R = rare earth; T = transition metal; X = p-block element) form what is perhaps the most varied set of intermetallic compounds known. They crystallize in many different structure types and exhibit an almost bewildering range of intrinsic magnetic and electrical behaviours. In a review of the RTX compounds by Pöttgen and Johrendt [3] it was noted that the 1-1-1 family encompasses 'more than 1000 representative compounds', crystallizing in 'about 40 different structure types'. If we consider only those 1-1-1 compounds that form with R = Eu, this review listed 72 compounds in 12 different structure types. In a subsequent paper, Müllmann *et al* [4] reviewed the properties of the EuTSn stannides, studied by ^{151}Eu and ^{119}Sn Mössbauer spectroscopy.

In this paper we focus on the magnetic structure of orthorhombic EuPdSn which has the TiNiSi-type structure (oP12). The space group is *Pnma* (#62) and all three atoms occupy 4c sites, generated by ($x\ \frac{1}{4}\ z$). The magnetic ordering temperature of EuPdSn was reported to be 13 K by Adroja and Malik [5]. The Eu ions were shown to be divalent on the basis of the increased cell volume compared to those isostructural compounds formed with other rare-earths. In a later paper, Müllmann *et al* [4] gave the magnetic ordering temperature as 15.5(5) K, determined by magnetometry measurements. A higher ordering temperature of 20.8 K was also reported, based on ^{151}Eu Mössbauer spectroscopy. Müllmann *et al* also reported seeing an anomaly at 6.0(5) K in their magnetometry measurements but we found no evidence in our work to support this. Müllmann *et al* confirmed the presence of Eu^{2+} ions by ^{151}Eu Mössbauer spectroscopy and they quoted a ^{151}Eu hyperfine field of 22.23(1) T at 4.2 K.

The magnetic ordering in many of the RPdSn stannides has been studied by neutron diffraction: Ce [6, 7], Pr [8], Nd [8], Tb [9–11], Dy [11, 12], Ho [11, 13, 14], Er [15]. Conspicuous by their absence from the neutron diffraction studies are Eu and Gd, due to their substantial neutron absorption. The thermal neutron absorption cross-section for natural europium is 4530 ± 40 b, while that of natural gadolinium reaches an enormous 49 700 ± 125 b, around 20 times that of cadmium; (these cross-sections are for a neutron wavelength of 1.8 Å. [16]). Neutron diffraction is by far the best method of determining a magnetic structure,

and studies of Eu and Gd compounds often resort to using 'hot' neutrons since the absorption cross-sections decrease with decreasing neutron wavelength. This option has the disadvantage of compressing the diffraction pattern into the lower 2θ angular range. Another, often expensive, option is to prepare samples using enriched isotopes with much lower absorption cross-sections, such as ^{158}Gd or ^{160}Gd. Recently, we have shown that satisfactory diffraction patterns for magnetic structure determinations can be obtained using a large-area flat-plate geometry [17], without resorting to short wavelengths or isotopically enriched samples, and examples of our recent use of this technique can be found in [18–22].

In this paper, we use the flat-plate technique to determine the complex magnetic order of the Eu sublattice in EuPdSn. To the best of our knowledge this is the first report of neutron diffraction measurements made on a ternary equiatomic EuTX intermetallic compound.

Figure 1. SEM image (back-scattered electron mode, accelerating voltage 20 kV) of the microstructure of EuPdSn annealed at 600 °C and water quenched (bright phase EuPdSn; dark phase, $EuPd_2Sn_2$).

2. Experimental methods

Starting materials for the preparation of the EuPdSn sample were europium [pieces, 99.99% Eu/TREM (trace rare earth metals) purity; Smart Elements GmbH, Vienna, Austria], palladium (foil, 99.95 wt% purity; Chimet, Arezzo, Italy) and tin (bar, 99.999 wt% purity). Owing to the fact that europium is sensitive to both air and moisture, the EuPdSn sample was prepared in a glove box. The sample, with a total mass of 2.6 g, was prepared by weighing stoichiometric amounts of the constituent elements. The elements were enclosed in a small tantalum crucible sealed by arc welding under pure argon, in order to avoid the loss of Eu due to its high vapour pressure. The sample was melted in an induction furnace, under a stream of pure argon. The resulting ingot was annealed in a resistance furnace at 600 °C for 3 weeks and finally quenched in cold water. After quenching, the sample was characterized by scanning electron microscopy (SEM) (Carl Zeiss SMT Ltd, Cambridge, UK), and electron probe micro-analysis (EPMA) based on energy dispersive x-ray spectroscopy. For the quantitative analysis, an accelerating voltage of 20 kV was applied for 100 s and a cobalt standard was used for calibration. The x-ray intensities were corrected for ZAF effects (atomic number–absorption–fluorescence). X-ray diffraction (XRD) patterns were collected at room temperature on an X'Pert MPD diffractometer (Philips, Almelo, The Netherlands) equipped with a graphite monochromator installed in the diffracted beam (Bragg–Brentano, Cu Kα radiation).

To prepare the flat-plate sample for the neutron diffraction measurements, 2.3 g (about a $1/e$ absorption thickness) was spread across a 2 cm × 8 cm area on a 600 μm thick single-crystal silicon wafer and immobilized using a 1% solution of GE-7031 varnish in toluene/methanol (1:1) [17]. Neutron diffraction experiments were carried out on the C2 multi-wire powder diffractometer (DUALSPEC) at the NRU reactor, Canadian Neutron Beam Centre, Chalk River, Ontario. The plate was oriented with its surface normal parallel to the incident neutron beam to maximize the total flux onto the sample and the measurements were made in transmission mode. A neutron wavelength (λ) of 1.3286(1) Å was used so that low-angle peaks due to any antiferromagnetic ordering would be well clear of any direct beam contamination. In order to ensure that no low-angle magnetic diffraction peaks were missed, an initial set of diffraction patterns was obtained with a longer wavelength of 2.37 Å.

Temperatures down to 3.6 K were obtained using a closed-cycle refrigerator with the sample in a partial pressure of helium to ensure thermal uniformity. All full-pattern magnetic and structural refinements employed the FullProf/WinPlotr suite [23, 24] with neutron scattering length coefficients for natural Eu taken from the tabulation by Lynn and Seeger [25]. No absorption correction was applied; however, the data were truncated at $2\theta = 51°$ to minimize the impact of angle-dependent absorption effects.

3. Results

In figure 1 we show a photomicrograph of the EuPdSn sample. EPMA reveals that the microstructure consists of a majority phase of composition EuPdSn with a small amount of an impurity phase with a stoichiometry corresponding to $EuPd_2Sn_2$. The XRD data confirm the formation of the EuPdSn phase TiNiSi structure type. A few tiny peaks probably belonging to the 1-2-2 impurity phase are also present.

In figure 2 we show a series of neutron diffraction patterns obtained on EuPdSn over the temperature range 20–3.6 K, at a neutron wavelength of 1.3286(1) Å. The appearance of purely magnetic peaks in the angular range $8° \leq 2\theta \leq 26°$ is clear.

In figure 3 we show the 40 and 3.6 K patterns, along with the difference between these patterns, emphasizing the appearance of strong magnetic peaks at low temperature. The downturn at the low-2θ end of the difference plot is due to the loss of incoherent scattering as the Eu moments order. In figure 4 we show the thermal variation of the intensities of selected magnetic diffraction peaks. The intensities of the strongest magnetic peaks yield a magnetic ordering temperature (T_N) of 16.2(3) K, in good agreement with

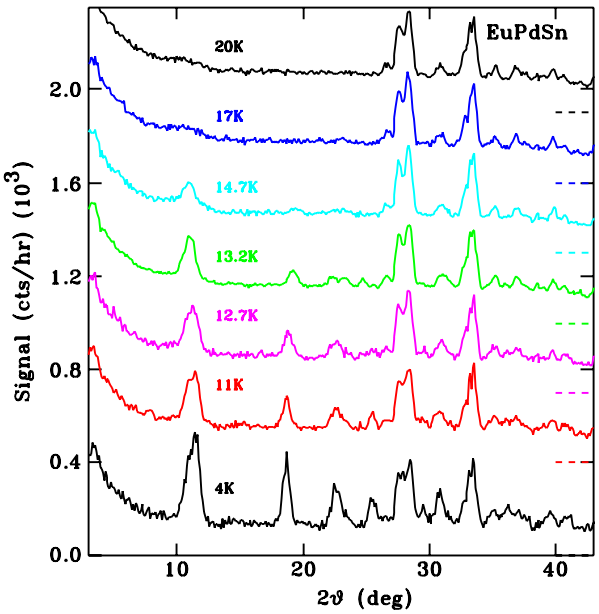

Figure 2. Neutron diffraction patterns of EuPdSn at various temperatures obtained using the flat-plate sample mount and $\lambda = 1.3286(1)$ Å.

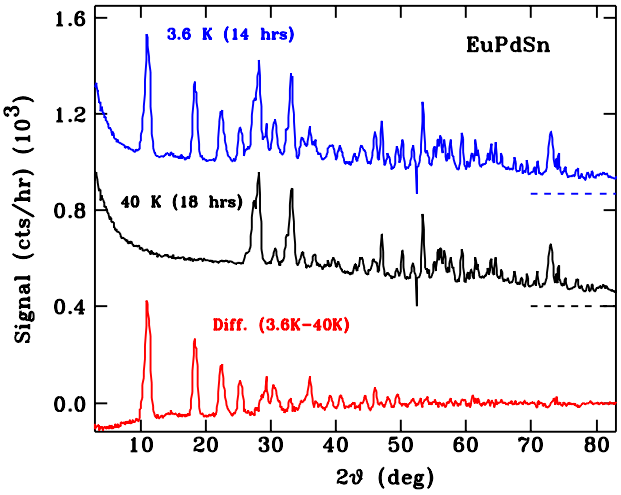

Figure 3. Neutron diffraction patterns of EuPdSn at 40 and 3.6 K, together with the difference between these two patterns. The 40 and 3.6 K patterns have been offset vertically for clarity and their respective baseline positions are shown by the dashed lines at the right.

previously reported values [4, 5]. It is also clear in this figure that there is a change in the magnetic structure of EuPdSn at around 12 K, as shown by the kinks in the intensity variations. In the lower panel of figure 4 we plot the thermal variations of the positions of selected magnetic peaks, once again emphasizing the change in magnetic structure around 12 K.

3.1. Neutron diffraction study in the paramagnetic state: $T = 40$ and 20 K

The refinement of the diffraction pattern taken at 40 K, well above the T_N of 16.2(3) K, is presented in figure 5 and clearly shows the nuclear Bragg peaks of the EuPdSn phase. The

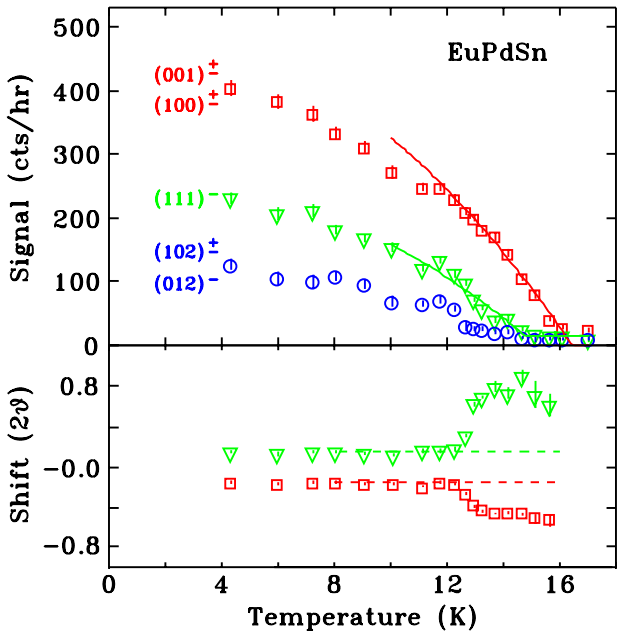

Figure 4. (Top) temperature dependence of the intensities of selected magnetic diffraction peaks. (Bottom) corresponding peak positional shifts, relative to 3.6 K, of selected magnetic peaks. (We have introduced small vertical offsets to distinguish the two curves.)

Table 1. Crystallographic data for EuPdSn obtained by refinement of the 40 K neutron powder diffraction pattern.

Atom	Site	x	y	z
Eu	4c	0.020(2)	$\frac{1}{4}$	0.683(1)
Pd	4c	0.287(2)	$\frac{1}{4}$	0.386(2)
Sn	4c	0.161(2)	$\frac{1}{4}$	0.068(2)
	a (Å)	b (Å)	c (Å)	
	7.473(3)	4.670(2)	8.015(4)	

crystallographic data for EuPdSn, derived from the refinement to the 40 K neutron diffraction pattern, are given in table 1 and are in good agreement with the results of a single-crystal study of EuPdSn by Pöttgen [26]. The conventional 'R-factors' for our refinement are R(Bragg) = 10.2, R(F) = 11.2, R(wp) = 3.61 and R(exp) = 1.56.

The pattern obtained at 20 K is shown in figure 6 and the presence of a very broad diffraction feature around $2\theta = 10°$ points to short-range magnetic correlations that persist above the magnetic ordering temperature determined by neutron diffraction, as shown in figure 4. This observation is consistent with the ^{151}Eu Mössbauer spectroscopy results [4] and demonstrates that these two techniques, neutron diffraction and Mössbauer spectroscopy, probe magnetic structures on quite different length scales.

3.2. Neutron diffraction study in the magnetic state: $T = 3.6$ K

The neutron diffraction pattern recorded at 3.6 K (figure 7) shows many additional, purely magnetic peaks which can be indexed by the propagation vector $\mathbf{k} = [0, 0.276(1), 0]$,

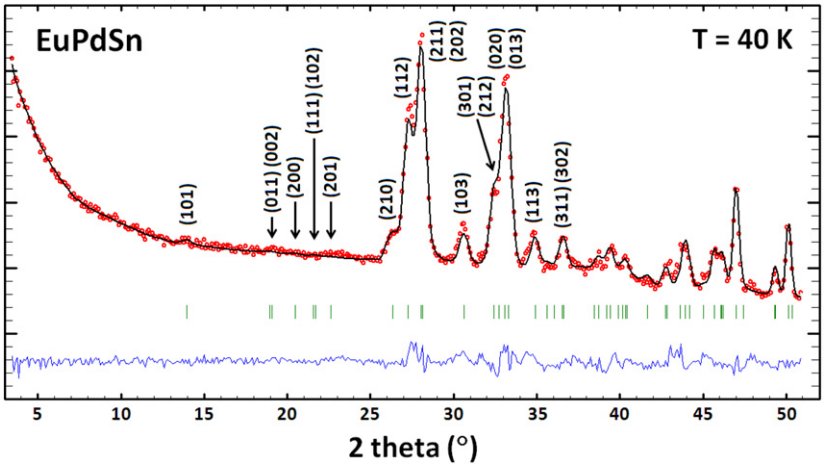

Figure 5. Refinement of the neutron powder diffraction pattern of EuPdSn obtained at 40 K with $\lambda = 1.3286(1)$ Å.

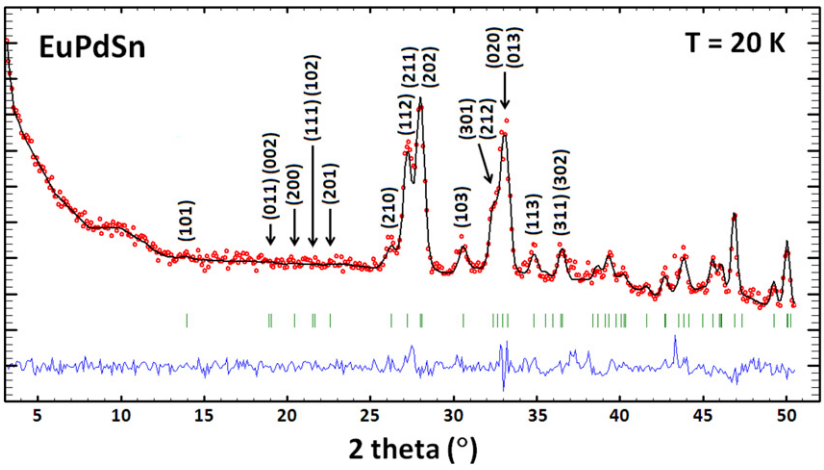

Figure 6. Refinement of the powder neutron diffraction pattern of EuPdSn obtained at 20 K with $\lambda = 1.3286(1)$ Å.

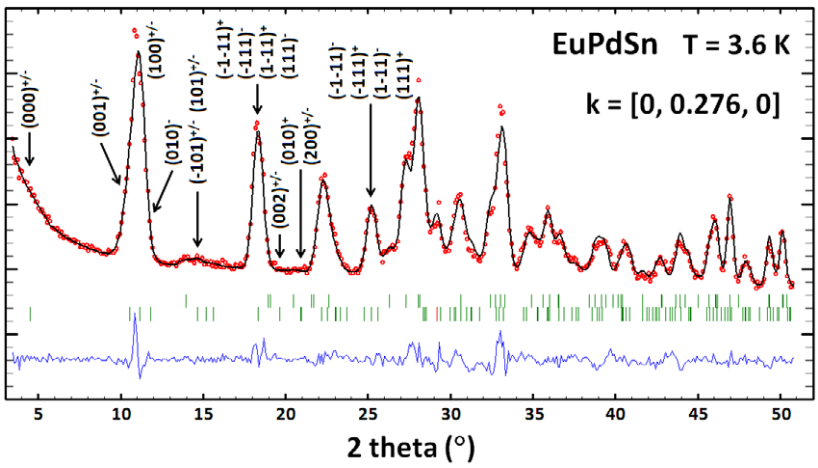

Figure 7. Refinement of the powder neutron diffraction pattern of EuPdSn obtained at 3.6 K with $\lambda = 1.3286(1)$ Å.

indicating an incommensurate antiferromagnetic structure. The absence of any magnetic contributions to the nuclear peaks allows us to exclude a conical magnetic structure. Furthermore, we can rule out a square-modulated magnetic structure from the absence of higher-order harmonic peaks.

The occurrence of the additional (00l) peaks with $l = 2n+1$ and (h00) peaks with $h = 2n+1$, which are forbidden by the crystallographic space group (*Pnma*), indicate a magnetic 'anti-a' mode. In this structure, the Eu atoms occupy a 4c site with the positions $(x;\ \frac{1}{4};\ z)$, $(-x;\ \frac{3}{4};\ -z)$, $(\frac{1}{2}-x;\ \frac{3}{4};\ z+\frac{1}{2})$

Table 2. Results from the various refinements of the 3.6 K neutron diffraction pattern of EuPdSn.

Parameter	Helimagnetic	Sinusoidal
a (Å)	7.476(3)	7.476(3)
b (Å)	4.673(2)	4.673(2)
c (Å)	8.008(3)	8.008(3)
x(Eu)	0.022(2)	0.022(2)
x(Pd)	0.287(2)	0.286(2)
x(Sn)	0.163(2)	0.163(2)
z(Eu)	0.682(1)	0.681(1)
z(Pd)	0.388(3)	0.388(3)
z(Sn)	0.073(2)	0.073(2)
Helimagnetic		
q_y	0.276(1)	
θ (deg)	90	
Magnetic phases (Eu_{1-4})	0; 0; 0.5; 0.5	
μ_{Eu} (μ_B)	6.60(6)	
Sinusoidal		
q_y		0.276(1)
$A(k)_{Eu}$		9.34(9)
θ (deg)		90
ϕ (deg)		45
Magnetic phases (Eu_{1-4})		0; 0.13(2); 0.63(2); 0.5
μ_{Eu} (μ_B)		6.60(6)
R(Bragg); R(F)	7.29; 5.63	7.28; 5.64
R(Mag)	6.23	6.39
R(wp); R(exp)	5.11; 1.80	5.11; 1.80
χ^2	8.08	8.07

and $(x+\frac{1}{2};\ \frac{1}{4};\ \frac{1}{2}-z)$, which we label Eu_1, Eu_2, Eu_3 and Eu_4, respectively. A magnetic 'anti-a' mode involves antiparallel magnetic coupling between Eu_1 and Eu_4, and between Eu_2 and Eu_3, leading to the two possible magnetic arrangements '$++--$' or '$+-+-$'. The absence of any magnetic intensity contributions to the $(0k0)$ reflections allows us to exclude the '$+\ -\ +-$' magnetic arrangement. Therefore, we conclude that the relative magnetic arrangement of the Eu moments in EuPdSn is '$++--$'.

The neutron diffraction pattern obtained at 3.6 K can be refined using either a planar helimagnetic ('flat spiral') structure or a sinusoidally modulated magnetic structure, and it is virtually impossible to distinguish between these two refinements. This is illustrated by the closeness of the various refinement R-factors for the two refinements, given in table 2, where we present the fitted parameters obtained in both refinements.

For the helimagnetic structure, the magnetic moments are oriented in the a, b plane ($\theta = 90°$) with a magnitude of 6.60(6) μ_B (table 2). For the sinusoidally modulated magnetic structure the magnetic moments are also oriented in the a, b plane ($\theta = 90°$) with an azimuthal angle ϕ (relative to the a-axis) of 45°. In the case of the sinusoidal modulation, the calculated intensities of the $(101)^{\pm}$ and $(\bar{1}01)^{\pm}$ peaks are higher than those observed experimentally. In order to reduce the intensity of these peaks we introduced a magnetic phase angle for the Eu_2 and Eu_3 atoms, relative to atoms Eu_1 and Eu_4. The best refinement is obtained with magnetic phases of 0, 0.13(2), 0.63(2) and 0.5 (in units of 2π) for the Eu_1, Eu_2, Eu_3 and Eu_4 atoms, respectively, and a sinusoidal magnetic amplitude $A(k)$ of 9.34(9) μ_B (table 2). The mean Eu magnetic moment (μ_{Eu}) in the sine-wave modulated magnetic structure is calculated from the amplitude $A(k)$ via the relation $\mu_{Eu} = A(k)/\sqrt{2}$. Hence, the mean Eu^{2+} magnetic moment at 3.6 K is 6.60(6) μ_B which is the same value as obtained with the planar helimagnetic structure and is close to the 'free-ion' value of 7.0 μ_B for the Eu^{2+} ion.

In order to distinguish between these two magnetic arrangements we note that the sinusoidally modulated magnetic structure yields a wide distribution of magnitudes of the Eu^{2+} magnetic moments. However, the ^{151}Eu Mössbauer linewidth at 4.2 K [4] is only slightly larger than the paramagnetic linewidth, which suggests that any distribution in Eu^{2+} moment is small, certainly less than 10%. Thus, we conclude that the planar helimagnetic ('flat spiral') structure is the correct magnetic structure in EuPdSn at 3.6 K.

This magnetic structure, shown in figure 8, is characterized by the rotation of the Eu magnetic moments in the (a, b) plane with the azimuthal angle ϕ_i (in degrees) calculated from the relation

$$\phi_i = (y_i \times q_y + \alpha_i) \times 360 \qquad (1)$$

where y_i is the y coordinate of the ith atom, q_y is the y component of the propagation vector $\mathbf{k}$ and α_i is the magnetic phase of the atom being considered. Thus the Eu_1, Eu_2, Eu_3 and Eu_4 atoms in the $i = 1$ crystallographic cell have rotation angles of 24.8°, 74.5°, 254.5°and 204.8°, respectively. From one crystallographic cell to the next the magnetic moment of a particular Eu atomic position (e.g. Eu_1) rotates by $q_y \times 360 = 99.4°$.

3.3. Neutron diffraction study in the magnetic state: $T = 13.2$ K

The neutron diffraction pattern recorded at 13.2 K (figure 9) shows magnetic peaks which can be indexed with the propagation vector $\mathbf{k} = [0, 0.217(2), 0]$ indicating an incommensurate magnetic structure. As in the case of the neutron pattern refinement at 3.6 K, the refinement of the 13.2 K pattern can be undertaken using either a planar helimagnetic ('flat spiral') structure or a sinusoidally modulated magnetic structure. However, unlike the situation at 3.6 K, the sinusoidal magnetic structure yields a clearly better refinement of the 13.2 K pattern, compared to that achieved using a planar helimagnetic structure, with a refined ϕ angle of 68(4)°(table 3) and magnetic phases of 0, 0.09(4), 0.59(4) and 0.5 for the Eu_1, Eu_2, Eu_3 and Eu_4 atoms, respectively. The refinement can be improved slightly by introducing a weak q_z component of 0.016(4), but the existence of such a weak modulation along the c-axis cannot be demonstrated unequivocally given the errors in the various refinement parameters and the signal to noise ratio of the diffraction pattern. We also considered an elliptical magnetic structure, comprising both a modulation and a rotation of the magnetic moments. This yields a refinement similar to that obtained with the sinusoidal structure. We found insignificant improvements

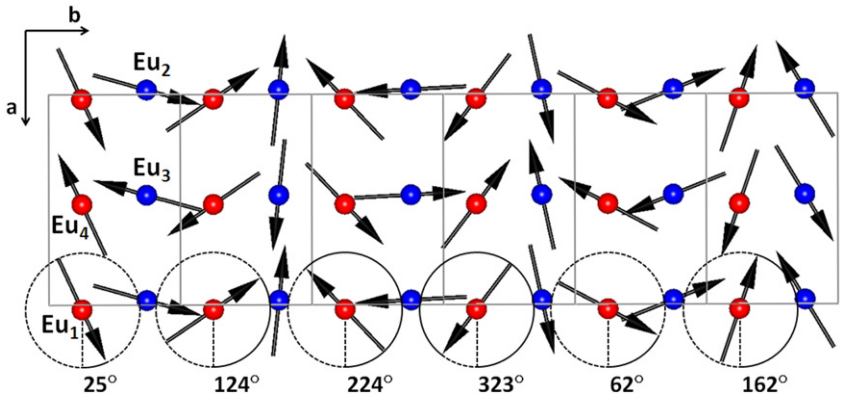

Figure 8. The planar helimagnetic ('flat spiral') structure of EuPdSn at 3.6 K. For clarity, we have omitted the non-magnetic Pd and Sn atoms.

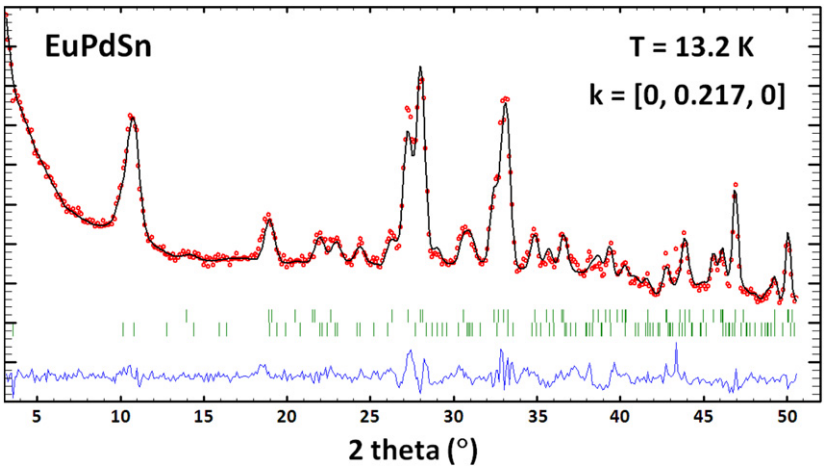

Figure 9. Refinement of the powder neutron diffraction pattern of EuPdSn obtained at 13.2 K with $\lambda = 1.3286(1)$ Å.

in the magnetic R-factor and χ^2 for the fit at the expense of a factor of four increase in the moment uncertainties, probably as a result of the increase in the number of fitted parameters. While we cannot exclude this elliptical structure, its complexity adds little to the analysis.

We therefore conclude that the magnetic structure of EuPdSn at 13.2 K is characterized by a propagation vector $\mathbf{k} = [0, 0.217(2), 0.016(4)]$ and a sinusoidal modulation of the Eu magnetic moment in the (a, b) plane with $\phi = 66(4)°$ and magnetic phases of 0, 0.08(4), 0.58(4) and 0.5 for the Eu_1, Eu_2, Eu_3 and Eu_4 atoms, respectively (table 3). The amplitude of the Eu^{2+} magnetic moment is 5.14(11) μ_B which leads to a mean Eu^{2+} magnetic moment of 3.63(8) μ_B. This sinusoidal magnetic structure is shown in figure 10.

4. Discussion

In the TiNiSi-type structure, the principal R–R magnetic couplings occur between the R_1 and R_2 atoms ($d = 3.745$ Å for EuPdSn at 3.6 K), which form zig-zag chains along the b-axis (figure 11), and between the R_1 and R_4 atoms ($d = 3.896$ Å for EuPdSn at 3.6 K), which form zig-zag chains along the a-axis (figure 11). At 3.6 K the Eu_1–Eu_4 and Eu_2–Eu_3 couplings are exclusively antiferromagnetic (figure 8) as a consequence of the magnetic 'anti-a' order. The Eu_1–Eu_2 and Eu_3–Eu_4 magnetic interactions comprise both ferro- and antiferromagnetic couplings (figure 8) resulting from the magnetic moment rotation $\phi_{1\to2}$ of 49.7°($=\frac{1}{2} \times q_y \times 360°$).

At 13.2 K the magnetic structure (figure 10) is characterized by a modulation of the magnetic moment with a period of 4.6 crystallographic cells along the b-axis, due to the $q_y = 0.217$ propagation component. There may also be a very weak modulation along the c-axis, but we cannot confirm this on the basis of the diffraction data. The deduced magnetic structure at 13.2 K shows exclusively antiferromagnetic Eu_1–Eu_4 and Eu_2–Eu_3 coupling from the magnetic 'anti-a' mode, and both ferro- and antiferromagnetic Eu_1–Eu_2 and Eu_3–Eu_4 couplings due to the magnetic moment amplitude modulation along the b direction (figure 10).

At 13.2 K, EuPdSn is characterized by an incommensurate sine-wave modulated (SWM) magnetic structure with a propagation vector $\mathbf{k} = [0, 0.217, 0.016]$. Such SWM magnetic structures have been observed for NdPdSn below $T_N = 3.6$ K ($\mathbf{k} = [0.273, \frac{1}{2}, \frac{1}{2}]$ at 1.5 K) [8], TbPdSn ($\mathbf{k} = [0, 0.25, 0]$) from $T_N = 19$ K to $T_S = 10$ K [9] and ErPdSn ($\mathbf{k} = [q_x \sim 0.32, \frac{1}{2}, q_z \sim 0.36]$) between $T_N = 5.2$ K and $T_t = 2.5$ K [15]. At 3.6 K, the magnetic structure of

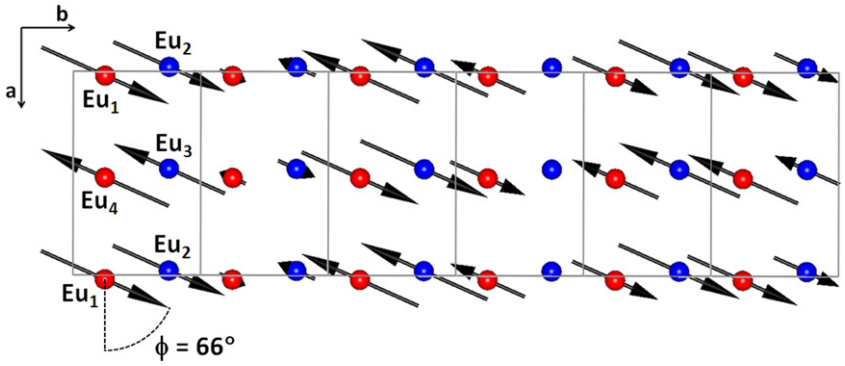

Figure 10. The sinusoidal magnetic structure of EuPdSn at 13.2 K. For clarity, we have omitted the non-magnetic Pd and Sn atoms.

Table 3. Results from the various refinements of the 13.2 K neutron diffraction pattern of EuPdSn.

Parameter	Helimagnetic	Sinusoidal	Sinusoidal	Sinusoidal
a (Å)	7.480(4)	7.480(4)	7.477(3)	7.477(3)
b (Å)	4.683(2)	4.683(2)	4.681(2)	4.681(2)
c (Å)	8.026(4)	8.026(4)	8.023(4)	8.022(4)
x(Eu)	0.023(3)	0.023(3)	0.022(3)	0.021(3)
x(Pd)	0.287(2)	0.287(2)	0.286(2)	0.286(2)
x(Sn)	0.163(2)	0.163(2)	0.163(2)	0.163(2)
z(Eu)	0.679(2)	0.679(2)	0.681(2)	0.681(2)
z(Pd)	0.391(3)	0.391(3)	0.391(3)	0.391(3)
z(Sn)	0.075(2)	0.075(2)	0.076(2)	0.076(2)
Helimagnetic				
q_y	0.220(2)			
θ (deg)	90			
Magnetic phases (Eu_{1-4})	0; 0; 0.5; 0.5			
$\mu_{Eu}(\mu_B)$	3.84(7)			
Sinusoidal				
q_y		0.220(2)	0.217(2)	0.217(2)
q_z		0	0	0.016(4)
$A(k)_{Eu}$		5.44(10)	5.06(10)	5.14(11)
θ (deg)		90	90	90
ϕ (deg)		45	68(4)	66(4)
Magnetic phases (Eu_{1-4})		0; 0.14(4); 0.64(4); 0.5	0; 0.09(4); 0.59(4); 0.5	0; 0.08(4); 0.58(4); 0.5
$\mu_{Eu}(\mu_B)$		3.85(7)	3.58(7)	3.63(8)
R(Bragg); R(F)	10.3; 10.2	10.4; 10.2	10.3; 9.99	10.1; 9.80
R(Mag)	23.1	23.7	16.6	16.2
R(wp); R(exp)	4.91; 1.88	4.90; 1.88	4.47; 1.88	4.45; 1.88
χ^2	6.81	6.80	5.67	5.64

EuPdSn is an incommensurate planar helimagnetic structure ('flat spiral') with a propagation vector $\mathbf{k} = [0, 0.276, 0]$. A similar propagation vector and magnetic arrangement ('$++--$') have been observed in TbPdSn [9], while a flat spiral magnetic structure was reported for CePdSn ($\mathbf{k} = [0, 0.473, 0]$) [6]. As we have demonstrated here, EuPdSn shows a thermal evolution of the magnetic structure which is sine-wave modulated below T_N and planar helimagnetic

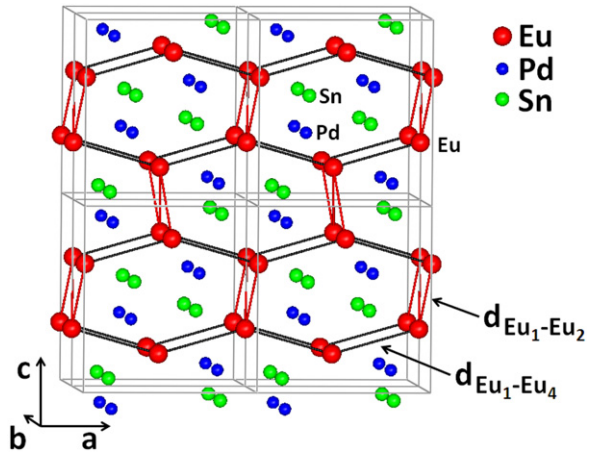

Figure 11. Illustration of the principal Eu–Eu magnetic interactions in EuPdSn.

at lower temperature, consistent with the divalent state of the Eu^{2+} Kramers ion for which one would expect a squaring of the modulation ('equal-moment') or a 'lock-in' transition to a commensurate phase [27–29]. This kind of magnetic transition, suggested by Rossat-Mignod [27], probably occurs around $T_t = 12$ K, the temperature below which the $(001)^{\pm}$, $(100)^{\pm}$ and $(111)^{-}$ magnetic diffraction peaks have effectively constant 2θ positions (figure 4). Similar magnetic transitions, from sine-wave modulation to an 'equal-moment' magnetic structure, have been reported for TbPdSn [9–11] and ErPdSn [15]. However, the low temperature magnetic structures of these compounds are in fact square-modulated, as deduced from the observation of higher-order harmonic peaks (**k** and 3**k**), while for the present case of EuPdSn, the absence of such harmonic satellites allows us to exclude a square-modulated magnetic structure.

5. Conclusions

The TiNiSi-type structure, antiferromagnetic ordering and divalent state of europium in EuPdSn have been confirmed by neutron powder diffraction. The magnetic ordering temperature is 16.2(3) K and the magnetic diffraction peaks at 13.2 K can be indexed with the propagation vector $\mathbf{k} = [0, 0.217, q_z]$ ($q_z \leq 0.02$). At 3.6 K, the propagation

vector is $\mathbf{k} = [0, 0.276, 0]$, indicating an incommensurate antiferromagnetic structure at both temperatures. At 13.2 K, the best refinement is obtained with a sinusoidally modulated magnetic structure with europium magnetic moments oriented in the (a, b) plane and an azimuthal ϕ angle of 66(4)°, relative to the a-axis. At 3.6 K, the neutron powder diffraction pattern can be equally well refined with either a sinusoidally modulated magnetic structure or a planar helimagnetic structure ('flat spiral'), with europium magnetic moments in the (a, b) plane for both magnetic structures. However, as expected at very low temperature for a Kramers ion, and supported by ^{151}Eu Mössbauer spectroscopy, the Eu^{2+} magnetic moments must have equal magnitudes, indicating an (a, b) planar helimagnetic structure at 3.6 K. Thus, the magnetic structure of EuPdSn is sinusoidally modulated below $T_N = 16.2(3)$ K and transforms into a planar helimagnet at lower temperatures (probably below $T_t = 12$ K). This is the first report of such a magnetic structural transition in the RPdSn series of compounds.

Acknowledgments

Financial support for various stages of this work was provided by the Natural Sciences and Engineering Research Council of Canada and Fonds Québécois de la Recherche sur la Nature et les Technologies. JMC acknowledges support from the Canada Research Chairs programme. Professor Marian Reiffers is gratefully acknowledged for providing the europium metal.

References

[1] Bauer E *et al* 2005 *J. Phys.: Condens. Matter* **17** S999–1009
[2] Carrretta P, Giovannini M, Horvatic M, Papinutto N and Rigamonti A 2003 *Phys. Rev.* B **68** 220404
[3] Pöttgen R and Johrendt D 2000 *Chem. Mater.* **12** 875–97
[4] Müllmann R, Ernet U, Mosel B D, Eckert H, Kremer R K, Hoffmann R D and Pöttgen R 2001 *J. Mater. Chem.* **11** 1133–40
[5] Adroja D T and Malik S K 1992 *Phys. Rev.* B **45** 779–85
[6] Kasaya M, Tani T, Ohoyama K, Kohgi M and Isikawa Y 1992 *J. Magn. Magn. Mater.* **104–107** 665–6
[7] Kadowaki H 1999 *J. Phys. Chem. Solids* **60** 1199–201
[8] Kolenda M, Baran S, Oleś A, Stüsser N and Szytuła A 1998 *J. Alloys Compounds* **269** 25–8
[9] André G, Bourée F, Oleś A, Sikora W, Kolenda M and Szytuła A 1993 *J. Magn. Magn. Mater.* **125** 303–9
[10] Kotsanidis P A, Yakinthos J K and Roudaut E 1994 *Solid State Commun.* **91** 295–9
[11] Andoh Y, Ingjie Z, Kurisu M, Nakamoto G and Tsutaoka T 2007 *ISSPNL Report* vol 14, University of Tokyo, p 74
[12] André G, Bourée F, Bombik A, Oleś A, Sikora W, Kolenda M, Szytuła A, Pacyna A and Zygmunt A 1994 *Acta Phys. Pol.* A **85** 275–8
[13] Andoh Y, Kurisu M, Nakamoto G, Tsutaoka T, Makihara Y, Kosugi T and Kawano S 2003 *Physica* B **327** 389–92
[14] Szytuła A, Oleś A, Penc B and Stüsser N 2004 *J. Alloys Compounds* **370** L14–6
[15] André G, Bourée F, Guillot M, Kolenda M, Oleś A, Sikora W, Szytuła A and Zygmunt A 1995 *J. Magn. Magn. Mater.* **140–144** 879–80
[16] Sears V F 1992 *Neutron News* **3** 26–37
[17] Ryan D H and Cranswick L M D 2008 *J. Appl. Crystallogr.* **41** 198–205
[18] Cadogan J M, Ryan D H, Napoletano M, Riani P and Cranswick L M D 2009 *J. Phys.: Condens. Matter* **21** 124201
[19] Ryan D H, Cadogan J M, Ritter C, Canepa F, Palenzona A and Putti M 2009 *Phys. Rev.* B **80** 220503(R)
[20] Ryan D H, Cadogan J M, Cranswick L M D, Gschneidner K A Jr, Pecharsky V K and Mudryk Y 2010 *Phys. Rev.* B **82** 224405
[21] Ryan D H, Cadogan J M, Xu S, Xu Z and Cao G 2011 *Phys. Rev.* B **83** 132403
[22] Ryan D H, Lee-Hone N R, Cadogan J M, Canfield P C and Bud'ko S L 2011 *J. Phys.: Condens. Matter* **23** 106003
[23] Rodríguez-Carvajal J 1993 *Physica* B **192** 55–69
[24] Roisnel T and Rodríguez-Carvajal J 2001 *Mater. Sci. Forum* **378–381** 118–23
[25] Lynn J E and Seeger P A 1990 *At. Data Nucl. Data Tables* **44** 191–207
[26] Pöttgen R 1996 *Z. Naturf.* B **51** 806–10
[27] Rossat-Mignod J 1987 *Methods of Experimental Physics* vol 23 (part C), ed K Sköld and D L Price (New York: Academic) chapter 19 (Magnetic Structures) pp 132–4
[28] Gignoux D and Schmitt D 1993 *Phys. Rev.* B **48** 12682–91
[29] Gignoux D and Schmitt D 2001 *J. Alloys Compounds* **326** 143–50